Analysis of the temperature dependent optical properties of V1−xWxO2 thin films

Abdelaziz Ait Abdelkadir, Jean-Louis Victor, Guillaume Vignaud, Corinne Marcel, Mustapha Sahal, Malik Maaza, Mohamed Chaker, Alain Gibaud

Version of Record: https://www.sciencedirect.com/science/article/pii/S0040609023001347
Manuscript_45f49184669ee59867dd2d25b7321f6b

Analysis of the temperature dependent optical properties of $V_{1-x}W_xO_2$ thin films

Abdelaziz Ait Abdelkadir [1,3,4], Jean-Louis Victor[2], Guillaume Vignaud[3], Corinne Marcel[2], Sahal Mustapha[4], Malik Maaza[5], Mohamed Chaker[6] and Alain Gibaud[1, *]

[1] IMMM, (UMR 6283 CNRS), Le Mans Université, 72085 Le Mans Cedex, France

[2] CEA, DAM, Le Ripault, F-37260 Monts, France

[3] Institut de Recherche Dupuy de Lôme (IRDL), UMR CNRS 6027, Université Bretagne Sud, Lorient, Cedex, France

[4] University of Ibn Zohr, ERMAM, FPO, Ouarzazate, 685324, Morocco

[5] Nanosciences African Network (NANOAFNET), iThemba LABS-National Research Foundation, 1 Old Faure Road, 7129, Somerset West, Western Cape Province, South Africa

[6] INRS Energie Matériaux Télécommunications, 1650 Lionel-Boulet Blvd, Varennes, Qc, J3X 1P7, Canada

Abstract

Vanadium dioxide is one of the most promising materials that can be used to control and tune in real time the optical properties of nanoscale devices due to its ability to perform a Metal-Insulator Transition (MIT). In this paper, we report the optical and structural properties of undoped and W-doped $V_{1-x}W_xO_2$ vanadium dioxide thin films deposited on oxidized silicon substrates using magnetron sputtering. The structural properties determined by X-ray diffraction showed not only the transition from a monoclinic to a rutile phase when crossing the metal–insulator transition temperature (T_{MIT}) but also a coexistence of phases for the tungsten-doped VO_2 even at room temperature. It is also shown that T_{MIT} decreases from 69.6°C to 41.6°C as x increases from 0 to 3%. A point-by-point fitting method is proposed to reliably extract the refractive index and extinction coefficient from spectroscopic ellipsometry measurements as a function of temperature and tungsten concentration. This approach avoids all the correlations between the thickness and the refractive index well known in

absorbent films calling into question the uniqueness of the results. The dielectric function is then calculated from the point by point refractive index. A model based on Tauc-Lorentz oscillators in the insulating phase to which a Drude component is added in the metallic phase provides information on the levels of the energy bands and the plasma frequency of the films. The calculation of reflectance and transmittance of $V_{1-x}W_xO_2$ thin films highlights the effect of W doping on thermochromic performance.

Keywords: *Spectroscopic Ellipsometry, X-ray reflectivity, X-ray diffraction, Point by point fit, VO2 thin films; Optical properties, W doping, Structural and electronic transition.*

1. Introduction

Vanadium dioxide is a material that crystallizes at room temperature in a monoclinic insulating phase (Space Group $P2_1/c$). It undergoes a Structural Phase Transition (SPT) to a metal tetragonal phase (Space Group $P4_2/mnm$) at about 68°C [1]. This transition called Metal Insulator Transition (MIT) has been widely studied since its discovery in 1959 by Morin [2]. At the transition, the electrical conductivity drastically drops when the temperature decreases. Simultaneously, the optical absorption, the dielectric and magnetic response are affected [3-5]. During SPT changes, the crystal structure undergoes large transformation strain. Unlike most other materials exhibiting MIT or SPT, in VO_2 these two transitions are intrinsically coupled and appear to occur simultaneously. This effect has fueled the long-lasting debate about the physics underlying the combined transition [6]. Different approaches were used to trigger the phase transformation such as thermal stimulation [2],

electrical stimulation "by current or voltage", pressure, strain [7] or by introducing defects into the VO_2 lattice [8]. A review of these approaches is available in the article by Shao et al. [9].

Despite the potential application of thin films of vanadium dioxide, their high MIT temperature T_{MIT} ~ 68°C is a clear limitation for the full exploitation of this potential. It is particularly interesting to be able to reduce the T_{MIT} close to room temperature. This will increase the functionality of VO_2 thin films and thus facilitate their integration into many devices such as optical switches and modulators, smart windows [10, 11], smart radiators, and IR and THz detectors [6, 12, 13]. To vary the critical temperature T_{MIT} of the MIT, doping is usually practiced. Depending on the material or the type of dopant, doping can be substitutional or interstitial. Electron donors (n type) such as W^{6+}, Mo^{6+}, Nb^{5+} [14-17] can efficiently reduce the transition temperature to room temperature, while doping by Ti [18], Si [19] or Ge [20] systematically shows an increase in this transition. In particular, W-doping was found to be one of the most effective strategy for reducing T_{MIT} resulting in a pronounced reduction in T_{MIT} of about ~20 K/at.%W for the bulk and by ~50 K/at.%W for the nanostructure [21-30]. Although several experimental investigations have been carried out on the diminution of T_{MIT} by W doping, there is still no unanimously accepted explanation of the mechanism involved. It is commonly accepted that the substitution of a V^{4+} ion by a W^{+6} ion induces disorder on the VO_2 host lattice or/and an increase in electron density in the conduction band of the VO_2 material.[15, 23, 26] It was initially suggested that the change in electron density does not affect the reduction in T_{MIT} and that only the change in structure is responsible. Indeed, Booth et al. [31] revealed by X-ray absorption fine structure of tungsten (VI)–doped vanadium dioxide in the insulating phase, and during the metal-insulator transition, that a large

expansion in the [110] and [$1\bar{1}0$] directions occurs through the phase transition from low to high temperature. This distortion breaks the bonds between Peierls-paired vanadium ions, opening a band gap, and reveals the nature of the mechanism by which tungsten doping lowers the transition temperature and enthalpy. These results suggest that a tetragonal structure forms around the W^{6+} ion and that this local deformation from monoclinic to tetragonal structure is responsible for the reduction of T_{MIT}. However, a characterization of the electronic contribution of the W^{6+} ion and its contribution to local structure modification by combining X-ray absorption fine structure and X-Ray Absorption Near Edge Structure measurements, demonstrated that these contributions are both responsible for the T_{MIT}.[23] Recent theoretical studies on transition and band structure have suggested an intermediate theory combining both Peierls and Mott, described in terms of Mott-assisted Peierls transition [32].

Although the MIT has been widely studied, there is still needs for the precise determination of the optical constants of VO_2 and *a fortiori* of $V_{1-x}W_xO_2$. Spectroscopic ellipsometry is the standard method to investigate the optical properties of thin VO_2 films. This technique provides the information about the refractive index across the characteristic MIT from ultra-violet to infrared frequency ranges [5, 33-38]. In our previous works [5, 33], we have analyzed by spectroscopic ellipsometry, the optical properties of pure VO_2 thin films. The analysis was carried out by fitting the ellipsometric datasets to a Drude-Lorentz model in the UV-visible range up to 4.5µm. Ellipsometry measurements have recently confirmed our results and others by extending the measurements in a wider range of wavelengths (300 nm to 30 µm) [36]. On the contrary, very little work on the ellipsometric analysis of the optical properties

of W-doped VO_2 is available. Recent studies have been reported on the analysis of ellipsometric measurements in Mo-doped VO_2 [32].

A common method of ellipsometric data analysis is to use dispersion functions to represent the refractive index of the VO_2 film and to adjust the dispersion parameters and thickness until satisfactory agreement is found between the calculated and experimental data. One of the problems to overcome when analyzing these properties is to find the right model to describe optical constants over a wide range of wavelengths. Correlations resulting from the absorbing nature of these films between the film thickness and the refraction index were observed [13, 39] as VO_2 exhibits broad absorptions even in its insulating phase. However, a point-by-point fit of the delta-psi ellipsometric measurements can be used alternatively to solve, wavelength by wavelength, the ellipsometric equations to determine two unknown parameters (refractive index n and extinction coefficient k) for each wavelength of the spectrum considered as a set of independent points [40]. Usually the point by point method is done in two steps: (i) the thickness of the film is determined with a simple dispersion function over a range of wavelengths where the film is transparent, (ii) this thickness is then fixed to independently determine at each measured wavelength the real and imaginary parts of the refractive index over the whole spectrum without requiring particular assumptions about the shape of a model dielectric function like in the traditional method of data fitting. In our study, X-ray reflectivity is used to accurately determine the thickness of the films. This allows us to constrain the film thickness in the point by point analysis of ellipsometric data which is an original approach in the studies of VO_2 thin films. The film thickness is indeed essential to analyze the ellipsometric data by the point by point method without any bias.

The main objective of this work is to extract the optical properties of thin films of

pure and tungsten-doped vanadium dioxide from point-by-point ellipsometric data analysis. Indeed, the optical properties of W-doped films deduced from ellipsometric analysis are not yet reported in the literature. This study is completed by X-ray diffraction and reflectivity studies to characterize the structure. X-ray diffraction shows how the structural transition occurs at low and high temperature in these films and how the hysteresis width is affected by W doping. Particular emphasis is given on the way to determine the percentage of monoclinic phase through the transition. X-ray reflectivity was then performed to analyze the thickness and the film roughness. The use of X-ray reflectivity is mandatory to fix the thickness of the films in the point-by-point analysis of the ellipsometric datasets. The point-by-point analysis of the ellipsometric data gives a reliable evolution of the real and imaginary parts of the refractive index of the VO_2 layer at each wavelength as a function of temperature and tungsten composition. By fitting with a Tauc-Lorentz model, the generated dielectric function deduced from the point-by-point analysis. We used a Tauc -Lorentz model to adjust the resulting dielectric function. A plot of the band structure based on the calculated energies of the inter-band transitions is provided. In addition, we report how the reflectance and the transmittance evolve in the UV-visible near infrared range.

2. Experimental details

W-doped VO_2 thin films have been prepared from the annealing of multilayers composed of VO_2/W bilayers. Layers were deposited on silicon substrate covered with an amorphous silicon oxide of 1.5 nm by a cylindrical sputtering device with a DP650 magnetron (ALLIANCE CONCEPT) [41]. Pulsed Direct Current Magnetron Sputtering (PDCMS) was used as the magnetron supply. The pulse repetition

frequency and duration were 50 kHz and 2 ms. VO_2 layers were deposited from a 75 mm diameter high purity (99.9% GENCOA) vanadium target in an Ar/O_2 environment. During the deposition process, Ar and O_2 gas flow rates were set at 60 sccm and 2.4 sccm, respectively for a total sputtering pressure of 1 Pa. A sputtering power of 250 W was used for each VO_2 layer deposition. W layers were deposited from a 150 mm diameter tungsten target (99.9% ALLIANCE CONCEPT) in an Ar discharge with a power supply set at 100 W. The Ar flow rate was set to 30 sccm for a total gas pressure maintained at about 0.7 Pa. The VO_2 and W thicknesses were adjusted in order to obtain multilayers with different (W/V) atomic ratios. Three different multilayers were deposited. The VO_2 and W thicknesses were adjusted in order to obtain multilayers with different (W/V) atomic ratios of 0.8 (Sample 1), 1.8 (Sample 2), 3 (Sample 3) respectively (Table 1). To ensure ultra-thin layers of W, dynamic mode deposition was used. The substrate holder was fixed on a rotating plate during the process. The deposition of W was carried out in several stages. First, power was applied on the W target to create the discharge while the substrate was positioned 180 ° from the W target. No deposition occurred during this first step. Then the rotating plate was activated to perform a full rotation allowing the deposition of a very thin film of W as the substrate moved under the W target. The rotation speed was adjusted according to the expected layer thicknesses of W. An annealing step at 450°C under Ar flow during 1 h was then carried out to allow the crystallization of VO_2 and the diffusion of W through the layers of VO_2. The heating and cooling rates were adjusted at 2°C/min and the Ar gas flow was set at 0.5 L/min throughout process.

The composition was determined by RBS (Rutherford backscattering spectrometry) with 2 MeV He ions at a scattering angle of 170° (see Table 1). The high energy ions

scattered by collisions involve Coulomb repulsion between the positively charged nuclei of the incident He ions and the target particles. The intensity of the RBS signal depends on the scattering cross-section, which is directly proportional to the square of the atomic number of the element. The distinct V signal combined with the W signal allowed the determination of the (W/V) atomic ratios of the film from simulated spectrum (Rutherford simulation program (SIMNRA) was used to simulate the RBS patterns). Note that for sake of clarity, the nominal concentration was used in the whole paper. For more details on the preparation of the samples see reference 41.

Table 1: Description of the different structure and W composition of the sputtered films.

	Pure	Sample 1	Sample 2	Sample 3
VO_2 thickness layer (nm)	74	22.5	15.0	15.0
Number of VO_2 layers	1	2	3	3
W thickness layer (nm)	0	0.08	0.14	0.21
Number of W layers	0	2	3	3
Nominal W content (%)	0	0.7	1.8	3
W content measured by RBS (%)	0	0.65	1.71	2.77
Total measured thickness (nm)	74	43	49.2	49.3

X-ray reflectivity measurements were measured at small angles between $2\theta=0°$ and $2\theta=6°$ using the Kα radiation from a copper anode mounted on an Empyrean reflectometer (Panalytical). The beam was made parallel using a toroidal mirror and the detector was reduced to almost a point detector by using 3 channels out of the 256 channels available. The incident beam was rectangular with a typical size

100µmx10mm. X-ray reflectivity data were analyzed with the reflex program [42]. The correction of geometrical factors was integrated in the program [43]. Reflectivity experiments were carried out in the θ-2θ mode after a careful alignment of the sample height and of the incident angle.

X-ray diffraction patterns were measured using the Empyrean diffractometer (Panalytical) between 2θ =20 to 60 degrees at 25°C and 85°C (the measurements were performed after a stabilization of the temperature for about 2 min and a heating rate 1°C/min) with the aim to both confirm the crystal structure of the film and to study the SPT. In this case, the PIXel3D detector was collecting the diffracted beam over a range of 3.35° using the 256 channels with 0.25° front slits and 0.5° back slits providing the best compromise in terms of signal/noise ratio. Diffraction experiments were carried out in the θ-2θ mode.

A spectroscopic ellipsometer JobinYvon−Uvisel instrument was used to measure the optical properties of all the films. It is mainly composed of a Xenon source, ranging from long-range infrared to ultraviolet (250-2100 nm), a polarizer, an analyzer, and a grating monochromator ensuring the dispersion and the selection of the wavelength to a detector. Two types of detectors are employed: photomultiplier for FUV-VIS range and InGaAs photodiode for NIR range. Both polarizers are held fixed during the measurement (configuration II: polarizer 45°, analyzer 0°) while the photoelastic modulator is used to induce a modulated phase shift of the reflected beam. The photoelastic modulator that can be described as a birefringence modulator is a fused silica bar exhibiting isotropic behavior when no stress is applied. The phase modulated ellipsometer delivers optimum accuracy for all values of Ψ and Δ ellipsometric angles (Ψ= 45°±0.01° and Δ=0°±0.01° measured in straight-through air configuration1.5 – 5.3 eV). This ellipsometer was equipped with a heating stage

(LinKAM TMSEL600) including a cover with spectroscopy grade quartz windows.

The acquired ellipsometric angles Δ and ψ of the VO_2 thin-film were collected for an incident angle α=70° from λ=275 nm to 1771 nm. The measurements were made at every 5°C interval from 25 to 85°C and before each measurement the sample was held at a fixed temperature for 5 min to achieve thermalization before starting the measurements. The rate of heating was 1 °/min between two measurements. The same procedure was followed for cooling.

The point by point methodology used to analyze the ellipsometric data is detailed in the Ellipsometric measurements section. First, the real and imaginary parts of the refractive index (respectively n and k) were determined by a fit to the measured ellipsometric parameters Δ and ψ at each wavelength. In a second step, we calculated the dielectric function from the n and k values. A Tauc-Lorentz oscillator model was then applied to extract the band structure of the tungsten doped VO_2 thin films.

3. Results and discussion.

3.1 X-ray reflectivity and X-ray diffraction.

X-ray reflectivity (XRR) is a technique that is used to analyze the electron density profile of thin films in the direction perpendicular to the film surface. A detailed description of this technique is provided in the following reference A. Gibaud & G. Vignaud [44]. Basically, XRR measurements consist of measuring the intensity reflected from the film as a function of the incident angle θ or as a function of the wave vector transfer $q_z=4\pi\sin(\theta)/\lambda$. In the analysis of the XRR data, films are broken down into a series of slabs with adjustable thickness, roughness and electron density. A three-layer model was applied to model the samples (see Table 2).

Table 2: Slab structure of the VO_2 films deposited on silicon

Slab	Silicon	SiO_2	VO_2
Thickness (*nm*)	∞	1.5	74
Roughness (*nm*)	0.2	0.2	2

The electron density of vanadium oxide and its thickness were defined as variables. The electron densities of silicon and native oxide were fixed to published values. The native oxide thickness was 1.5 nm. The combination of all these parameters gives the electron density profile (EDP) fitted to the experimental data (see insets of Fig. 1). XRR measurements were carried out above and below the transition temperature in order to follow the evolution of the film thickness since this parameter is of paramount importance for ellipsometric analysis.

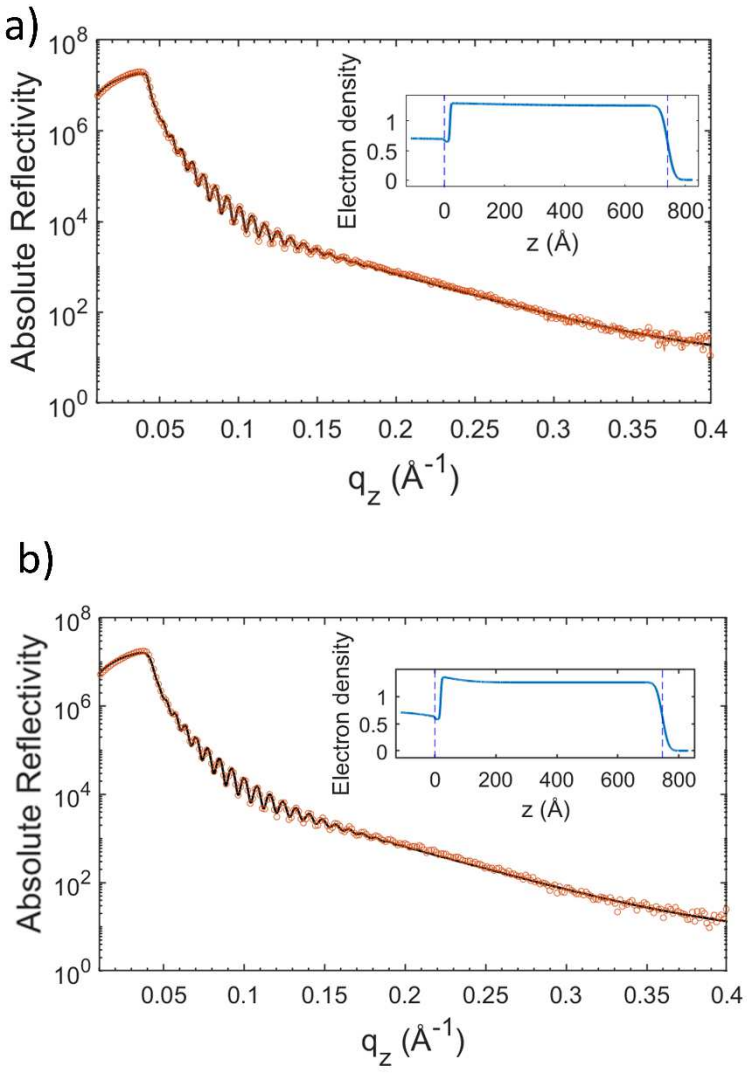

Fig. 1. Observed and calculated X-ray reflectivity of the pure VO_2 film at T=25°C (a) and 85°C (b). The inset in these figures shows the EDP.

Fig. 1 shows the X-ray reflectivity curves for the pure vanadium dioxide film at T=25°C (a) and T=85°C (b). A series of well-defined equidistant Kiessig fringes is observed up to 0.2 Å^{-1} consistent with a total thickness of the film close to 72 nm. The top roughness of the film was found to be of the order of 2 nm in agreement with the disappearance of the Kiessig fringes at higher q_z. From these measurements, it was found that the thickness of the film does not change much

during the transition. The same method was applied to the tungsten doped thin films x=[0.7%-1.8%-3%] at 25°C and the results are presented in Table 3. The doped films were found to be rougher than the pure film.

Table 3. Thickness and roughness measurements of pure and tungsten doped [0.7%-1.8%-3%] films at room temperature

VO_2	Pure	0.7%W	1.8%W	3%W
Thickness (nm)	74.0(4)	43.0 (3)	49.2(3)	49.3(3)
Roughness (nm)	2	3.32	4.2	4.6

X-ray diffraction patterns for both confirming the crystal structure of the film and studying the SPT are shown in the top panel in Fig. 2. A fit to the data was performed without any preferred orientation showing that these film are powder-like (see bottom panel in Fig. 2). We can therefore certainly consider that these films are made up of crystallites distributed randomly. The two diffractograms differ slightly in the position of the Bragg peaks. This is the signature that the phase transformation involves only slight displacements of atoms during the heating process.

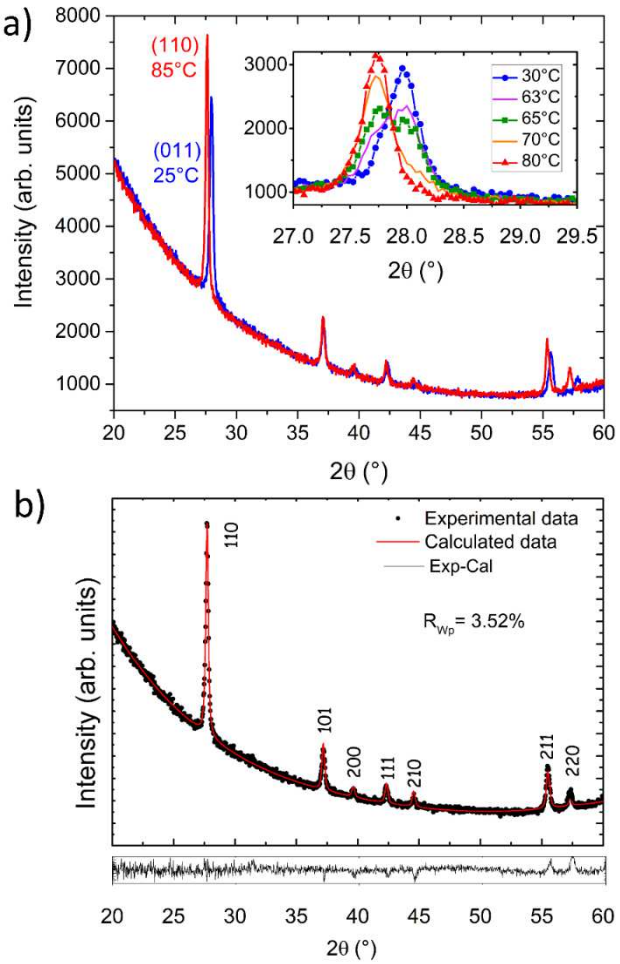

Fig. 2. a) Top panel: Diffractograms of pure VO_2 at T=25°C (blue curve - Monoclinic phase) and T=85°C (red curve-Rutile phase). The inset shows the coexistence of the (110) rutile reflection with the (011) monoclinic reflection through the transition (63-65°C). b) Bottom panel: fitting to data in the tetragonal phase using the MAUD program [45].

In particular, the strongest Bragg peak of the monoclinic phase located at 2θ = 28.0° shifts slightly to lower 2θ° values while others do not change much in position. This peak which is the (011) Bragg reflection of the monoclinic phase is transformed on heating into the Bragg (110) reflection of the rutile phase. The lattice parameters in both phases were determined by fitting to the data using the MAUD software [45]

and are shown in Table 4.

Upon cooling, a structural distortion occurs at the transition and the V-V pair changes from alternating V-V distance of 2.85 Å along the c_R axis to 3.28 Å and 2.36 Å along the a_m direction of the monoclinic phase (see Figure 3). The space group of VO_2 is transformed from $P4_2/mnm$ in phase R to $P2_1/C$ in phase M. This induces on cooling a doubling of the unit cell volume (see Table 4). The result agrees well with previous reports.[46-48]

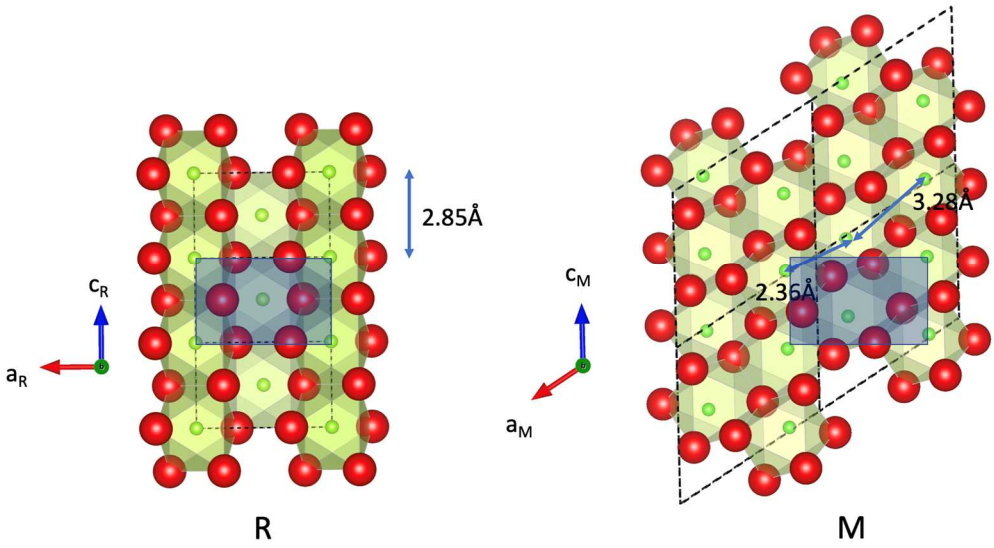

Fig. 3. Illustrations of crystalline structures of high-T Rutile Metal (R) and low-T Monoclinic (M) insulator phases of VO_2. The initial rectangular unit cell of the rutile phase is highlighted in blue on the left and right parts of the figure. The dashed lines describe the unit cells in both phases. Blue arrows on the right panel give the interatomic distances between consecutive vanadium ions along the [100] direction of the monoclinic unit cell.

Table 4. Calculated values of the lattice parameters of the two phases deduced from fits to the X-ray datasets using the MAUD program[45]. Errors are given in parenthesis.

Lattice parameters	Monoclinic	Rutile
a (Å)	5.749(1)	4.545(1)
b (Å)	4.492(2)	4.545(1)
c (Å)	5.366(4)	2.8517(3)
α	90	90
β	122.31(5)	90
γ	90	90
V (Å^3)	117.13	57.12

The shift of the monoclinic (011) peak was monitored as a function of temperature to gain a better understanding of the structural phase transformation occurring at the transition. The transition being of the first-order, the monoclinic (011) Bragg peak located at 2θ=27.75° coexists in a limited range of temperature with the rutile (110) Bragg peak located at 2θ=28.03° (see Fig. 4). By adjusting the peak intensity with fixed 2θ positions and widths of the Bragg peaks in the monoclinic and rutile phase, it is possible to estimate the percentage of the monoclinic phase in the film during the SPT.

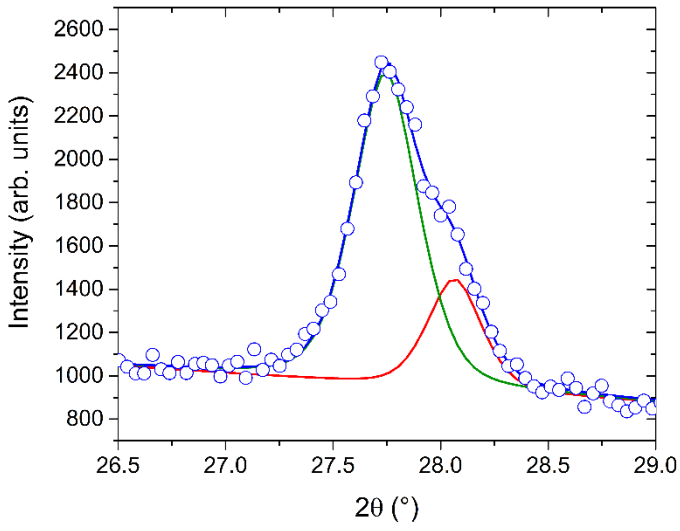

Fig. 4. Coexistence of the two Bragg peaks (011) of M phase (green) and (110) (red) of R phase measured at T=67.2°C on cooling. Observed (open circles) and calculated (blue line) data.

Figure 5 shows the well-known hysteresis that characterizes the MIT transition. The percentage of monoclinic phase further noted *f* was calculated as follows:

$$\%\, Monoclinic = f = \frac{I_{011}}{I_{011}+I_{110}} \quad (1)$$

where I_{011} and I_{110} intensities are the integrated intensities of the (011) and (110) Bragg reflections of the monoclinic and rutile phases after background removal.

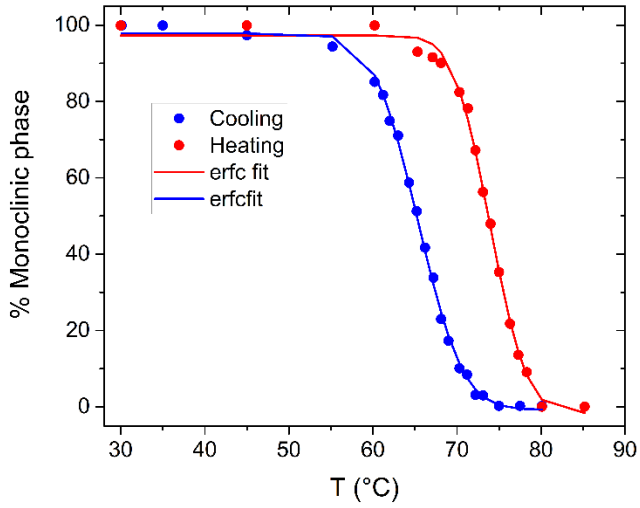

Fig. 5. Hysteresis of pure vanadium dioxide determined after integrating the intensities of the (011) and (110) Bragg reflections of the monoclinic and rutile phases. Solid lines are fit to the experimental data with the erfc function from equation (2).

In Fig. 5, we see that VO_2 transforms from a monoclinic phase to a rutile phase at a temperature of T_h= 73.9°C (red) upon heating and from a rutile phase to a

monoclinic phase at T_c=65.4°C (blue) upon cooling. The transition temperatures during the heating and cooling cycles (T_h and T_c) were determined from the fit to the data with a complementary error function (erfc) according to the equation [49]:

$$f(T) = \left(\frac{f_l + f_h}{2}\right) + \left(\frac{f_l - f_h}{2}\right) erfc\left(\frac{\sqrt{2}(T - T_0)}{\sigma}\right) \qquad (2)$$

where f_l and f_h are the asymptotic values of the monoclinic percentage in the low and high temperature ranges respectively and T_0 is the temperature at which the transition occurs (i.e., at which the function f (T) reaches 50% of its change), corresponding to either T_h or T_c for the heating or cooling cycles, respectively. The parameter σ is related to the width of the temperature interval around the T_0. The solid lines in Fig 5 and 6 are the best fits obtained with equation (2). The temperatures T_h and T_c correspond to a hysteresis of 9°C with a critical temperature defined by $T_{MIT} = (T_c + T_h)/2 = 69.6°C$ [50]. The phase transition is reversible as a function of temperature. However, recovering 100% of the monoclinic phase requires cooling down the film well below the transition temperature. The same method was applied to films doped with tungsten. It is clearly observed in Fig. 6 that doping by tungsten decreases the transition temperature.

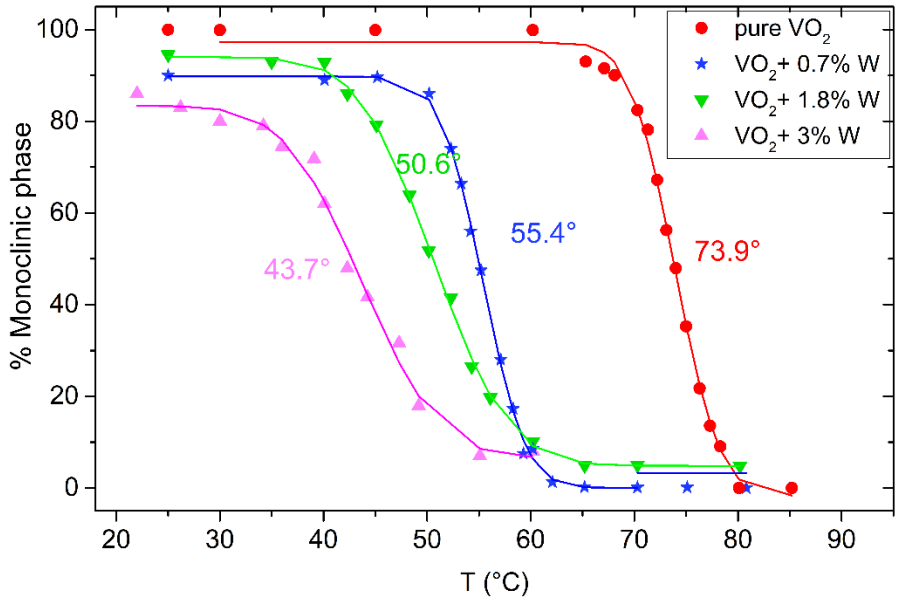

Fig. 6. Percentage of the monoclinic phase calculated from equation (1) upon heating for the $V_{1-x}W_xO_2$ films. Solid lines are fit to the experimental data with the erfc function from equation (2). The cooling cycle is not shown to avoid overloading the figure.

Upon heating, the transition temperature goes from T_h =73.9°C for pure VO_2 to T_h =55.4°C, 50.6°C and 43.7°C for x= 0.7%, 1.8% and 3% respectively. The critical temperature and the differential curve of the hysteresis loop are shown in Table 5.

Table 5. Critical temperature and ΔT_{MIT} of pure and tungsten doped [0.7%- 1.8%- 3%] films. T_h and T_c are the transition temperature on heating and cooling respectively. σ_h and σ_c are the temperature widths over which the transition occurs. Uncertainties on the last digit are given in parenthesis.

$W_xV_{1-x}O_2$	0%	0.7%W	1.8%W	3%W
Thickness (nm)	74.0(4)	43.0(3)	49.2(3)	49.3(3)
T_h (°C)	73.9 (2)	55.4 (2)	50.6 (2)	43.7(2)

σ_h	6.5 (3)	6.5 (3)	11.5 (3)	11.8 (3)
T_c (°C)	65.4 (2)	48.9(2)	42.3(2)	39.5(3)
σ_c	8.5 (3)	12.7 (3)	11.7 (3)	17.9 (3)
T_{MIT} (°C)	69.6	52.1	46.5	41.6
ΔT_{MIT} (°C)	8.5(5)	6.5(5)	8.3(5)	4.2(6)

The transition temperature during the cooling decreases from T_C=65.4°C to T_C=41.6°C. The width of the hysteresis loop varies from ΔT_{MIT} =8.5°C for pure VO_2 to ΔT_{MIT}=4.2°C when x increases from 0 to 3% respectively.

Note that the width of the hysteresis loop is affected by many factors such as grain boundaries, grain size, distribution and density of defects. For pure VO_2, it has been shown that the width of the hysteresis loop [49] gradually increases as the thickness of the VO_2 layer decreases. It is proposed that this phenomenon could be related to the formation of VO_2 crystallites during the deposition process with smaller and randomly oriented domains. Hysteresis cycles exhibit a width inversely proportional to the VO_2 crystallite size [51]. It is reported that the width varies from few degrees (2°C) in single crystals, up to few tens of degrees in thin films containing small nanocrystals with different sizes [52]. Hence, the width ΔT_{MIT} of our pure VO_2 film is in agreement with a polycrystalline film. The role of W doping on the width of the hysteresis cycle has been discussed by several authors [29, 53-56]. They observed that an increase of % W has the ability to reduce hysteresis width. Transitions in W-doped VO_2 show gradual transformation over a larger temperature range in contrast

to phase transition in undoped VO_2. This is consistent with our results which show a strong decrease of ΔT_{MIT} at 3% of tungsten and an increase of the parameter σ which measures the slope of the transition.

In Fig. 6, it is also interesting to observe that increasing the percentage of tungsten leads to a reduction of the monoclinic phase (100% to 83%) at 25°C when x varies from 0% to x=3%. This locally reflects a rutile structure around W dopants at 25°C (even at low doping concentrations) such as the V atoms in the R phase of VO_2 at high temperature[23]. At room temperature, the crystal structure of the doped VO_2 samples gradually shifts from M phase to R phase with increasing W concentration lowering the associated T_{MIT}. A similar but less pronounced effect is seen in the rutile phase as x increases.

Tang et al.[57] considered that the structural reason why the temperature is reduced is believed to be related to the destabilization of the V-V bonds by tungsten ions. The W^{6+} ion causes the rupture of the bonds between the V^{4+} -V^{4+} dimers and leads to the formation of W^{6+} -V^{4+} and V^{4+} -V^{3+} bonds. This causes a modification of the local structure around the tungsten atom and destabilizes the monoclinic structure of VO_2. Tungsten doping therefore reduces the energy barrier necessary for the transition to the tetragonal structure and facilitates the phase transition. [58]

3.2 Optical properties of pure VO_2 films

3.2.1 Data analysis methodology.

Ellipsometry is an optical characterization technique based on the analysis of the change in the state of polarization of a light wave after its reflection on the sample. A problem commonly encountered in ellipsometry is to determine the unknown refractive index and thickness of a thin film on a reflecting substrate with known

optical constants. By measuring the change in polarization state, i.e., psi (Ψ) and delta (Δ), of the light reflected from the sample at a fixed angle of incidence (AOI=70°), point-to-point fitting based on a two-layer model (VO_2 layer on top of an oxidized silicon substrate) can be used provided that the film thickness and the optical properties of the substrate are known. In our case, the fixed known parameters are the thickness of the silicon oxide which was determined to be 1.5 nm before film deposition, the wavelength dependent complex refractive index of the silicon and silicon oxide, the thickness of the VO_2 thin film and the incident angle fixed at 70°. At a given wavelength the measured parameters Δ and ψ which correspond to the change in amplitude and phase of the reflected light are only function of n and k. In the point-by-point fitting, at each wavelength, the knowledge of the two measured values Δ_{exp} and Ψ_{exp} becomes sufficient to yield a unique set of the two parameters n and k as the number of unknowns (n and k) is exactly equal to the number of ellipsometric equations. One set of (n, k) is searched such that the calculated Ψ_{cal} and Δ_{cal} are closest to the experimental Ψ_{exp} and Δ_{exp} by a numerical minimization of a residual function $\chi^2 \cong \left|\Delta_{cal} - \Delta_{exp}\right|^2 + \left|\psi_{cal} - \psi_{exp}\right|^2$ using a Levenberg-Marquard algorithm (LMA). The parameters Ψ and Δ can be exactly calculated by the matrix technique [42].

As the ellipsometric equations are highly nonlinear, it should be noted that in the point by point method, the initial values used in the fittings play a critical role [40] because LMA may get stuck in a local minimum which is not necessarily the global minimum. To prevent this difficulty, we started our fits from our previous data for pure VO_2 [5]. For doped VO_2 film, we first fitted the data to the conventional method (Lorentz-Drude oscillators with a film structure modeled using three layers: an effective medium approximation (EMA) layer for roughness on a homogeneous VO_2

layer on a SiO_2 layer (1.5 nm) on a Si substrate). We have also checked that the calculated (n, k) values were not in a local minimum by a multi-start program using different initial values. Another possible source of bias in the point-by-point approach could come from not taking into account the roughness of the VO_2 film (this would add 2 unknowns: the thickness of the rough layer and a void percentage). In order to estimate the influence of roughness, we generated simulated parameters Δ_{sim} and ψ_{sim} from a model consisting of a homogeneous VO_2 film 72 nm thick with a roughness of 5 nm and a vacuum mixture at 50%. The incident angle was set to 70° and the refractive index of the VO_2 film was modeled using a Drude Lorentz relation. From these simulated Δ_{sim} and ψ_{sim} we have extracted n and k by the point-by-point method considering a roughness-free film 77nm thick. In Fig. 7, the values of n and k resulting from these two calculations are compared. We see that the refractive index obtained by the point-by-point method is very close to that resulting from the simulation despite the fact that the roughness was not taken into account. As the roughnesses of our films remain below 5 nm, it can be assumed that the refractive indices calculated by the point-to-point method are not drastically biased.

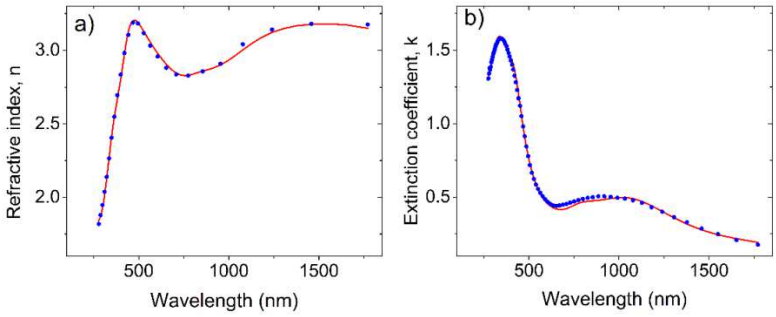

Fig 7. Comparison of refractive index a) and extinction coefficient b) calculations made from a 72 nm VO_2 film with **5 nm roughness** (red line) and a 77 nm film **without roughness** (blue symbols). See text for more details.

3.2.2 Refractive index and permittivity of pure VO_2 films

The point by point model directly provides a unique value of the real and imaginary parts of the refractive index for a given wavelength. Fig. 8 shows the fits of the measured Δ and Ψ of the film at each wavelength for the pure VO_2 film. One can see that the point by point approach leads to a quasi-perfect estimation of Ψ and Δ as shown by the difference between calculated and experimental data remaining well below 0.002°.

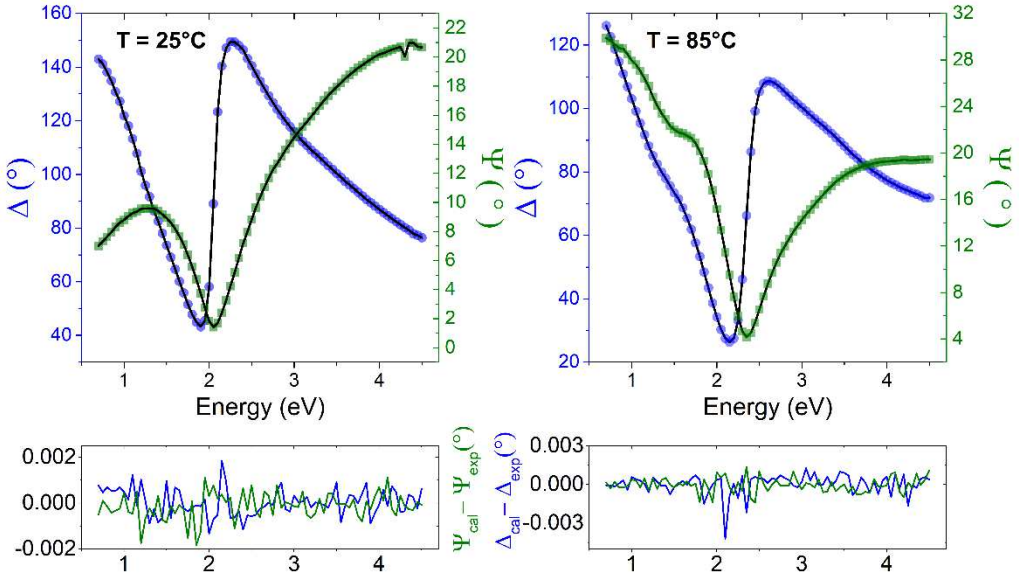

Fig 8. Top panel: Ellipsometric angles Ψ and Δ and the corresponding point-by-point-fit (black line) for pure VO_2 at 25°C and 85°C measured at an AOI=70°. Bottom panel: difference between the experimental and adjusted values for better observation of agreement.

We report in Fig. 9 (a-b) the evolution of the real and imaginary parts of the refractive index of the film at T=25°C and T=85°C, i.e. in the insulating and metallic phases. First, we observe that the symbols (squares and triangles) resulting from the point-by-

point method are evolving smoothly from one wavelength to the next, even though they were calculated independently. This is evidencing that the point by point refractive index calculation is robust. Second, the curves calculated by the classical method using a dispersion Drude-Lorentz oscillator function and by the point-by-point method are in good agreement. A slight difference in *n* at 85°C in the infrared range is nonetheless seen. This could be due to the broad absorptions of VO_2 in this energy range. Indeed it is observed (see Fig. 9) that the refractive index varies greatly in the infrared region as reported in several studies [5, 34-36]. At 85°C, the real part of the refractive index strongly decreases from 500 nm to 1700 nm while the extinction coefficient increases strongly in agreement with the expected metallic behavior of the film. In particular, at 1700 nm, the extinction coefficient increases by more than an order of magnitude. Such a lack of transparency can generate a difficulty in the data analysis since the use of a dispersion law means that the variation of any parameter can affect the calculation of the whole spectrum.

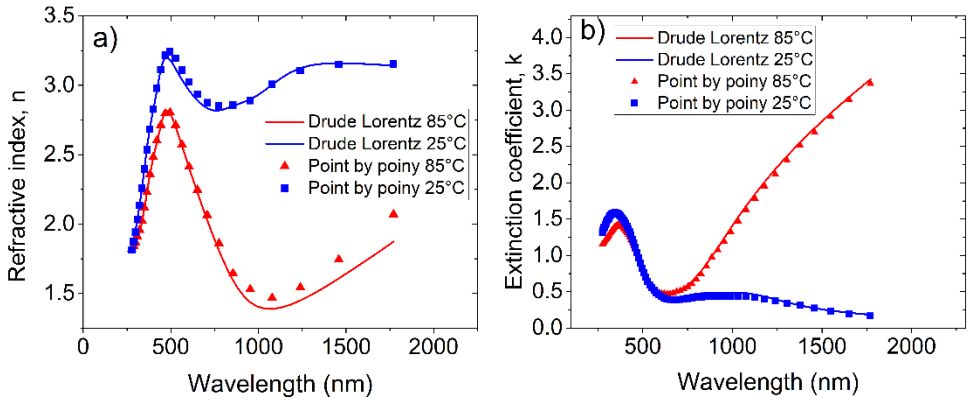

Fig. 9. Real (a) and imaginary parts (b) of the refractive index as a function of the wavelength at T=25°C and T=85°C.

The refractive index and the extinction coefficient of the film are plotted in Fig. 10 (a-b) as a function of temperature at three wavelengths. The real and imaginary parts of the refractive index vary more significantly at 1459 nm than at 497 nm as expected. Note that the hysteresis deduced from the analysis of the refractive index as a function of temperature is in excellent agreement with that observed by X-ray diffraction.

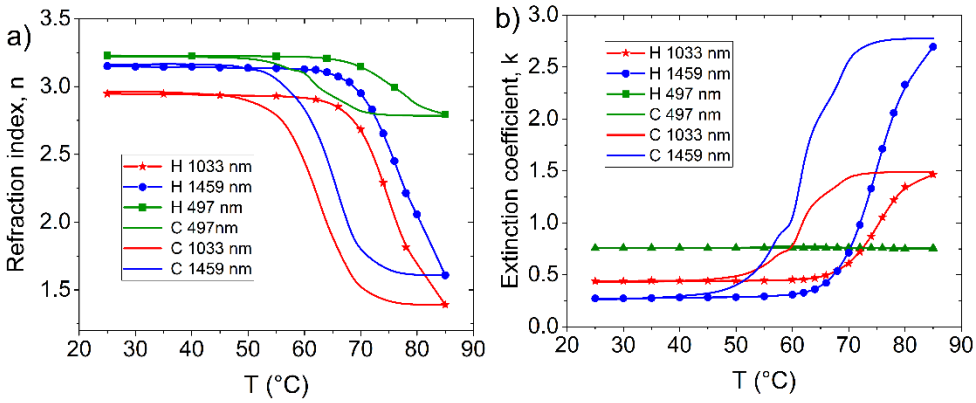

Fig. 10: Real (a) and imaginary parts (b) of the refraction index plotted versus temperature at three different wavelengths. (H stands for heating and C for cooling)

The real and imaginary parts of the dielectric function can be calculated from the complex value of the refractive index according to the following relationship:

$$(n + ik)^2 = Re(\varepsilon) + iIm(\varepsilon) \qquad (3)$$

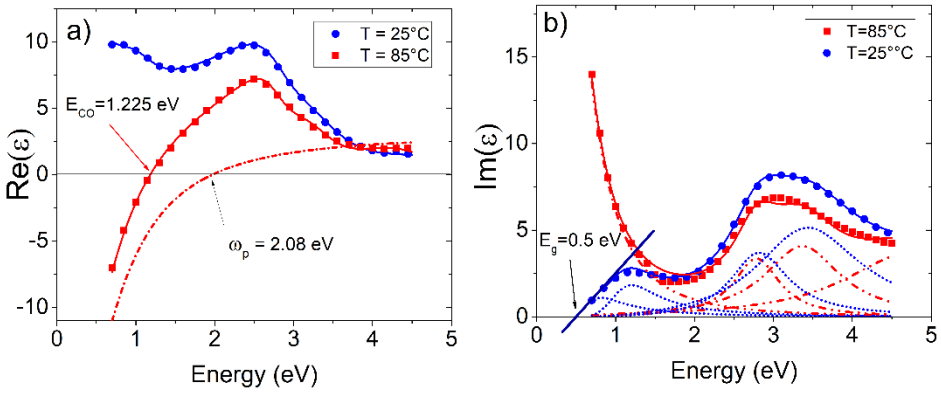

Fig. 11. Real (a) and Imaginary (b) part of the dielectric function below (in blue) and above (in red) the critical temperature for pure VO_2 thin films as a function of energy. The solid lines result from a fit with the Tauc-Lorentz model of the point by point dielectric functions. Dotted and dash-double-dotted lines show the different components used to fit the data in b) and dash-dotted line the contribution of the Drude function+ $\varepsilon_r(\infty)$ at 85°C in a) which crosses zero at the screened plasma energy ω_p.

In Fig 11b, the imaginary dielectric function of the insulating films shows an absorption in the near infra-red, at 0.8 eV and a broad absorption peak from 2 to 5 eV. At 25°C, the real part of the dielectric function is always positive while the imaginary part falls almost linearly to zero in the energy range from 1 eV to 0.5 eV. Interestingly, the intercept of this line at $Im(\varepsilon) = 0$ provides a rough estimate of the energy gap as described by Di et al.[59] The value here is 0.5 eV which is comparable to what is usually reported, i.e. 0.35 eV[38], 0.45 eV[37], 0.6 eV to 0.65 eV [9, 60, 61]. Note that this value strongly depends on the deposition conditions of the thin film as indicated by Jiang et al.[62] A smaller value (0.44 eV) resulting from stresses coming from the substrate is given by Nazari et al.[37]

The metallic behavior of VO_2 is characterized by a negative value of the real part of the dielectric permittivity due to the influence of the Drude function (for more details see references [33], [63]). The Drude part of the dielectric function brings a negative contribution to Re (ε) which tends to cancel the effect of the Lorentz part. The cross-over corresponding to the energy where the real part of the dielectric permittivity is zero in Fig. 11a, occurs at an energy E_{co}=1.225 eV for T=85°C. E_{co} is the screened plasma frequency, leading to a longitudinal wave solution of Maxwell's equation at

this energy. The plasma frequency of the free electrons (in the absence of bound electrons) would be 2.08 eV (defined by the zero of the Drude term), but this gets screened by the bound electrons and therefore reduced to 1.225 eV.

This energy would correspond to the screened plasma energy for free electrons. However, in VO_2 at 85°C, both the free electrons and the electrons participating to inter-band transitions contribute to the dielectric constant. The energy E_{co} at which Re(ε) goes through zero is not the plasma frequency ω_p defined by the zero of the Drude function (dashed line in figure 11a) but rather the energy at which the total permittivity cancels. Below E_{co}, the dielectric function is mostly imaginary and VO_2 behaves like a good conductor while above E_{co}, the film is more transparent that is to say weakly absorbing. It can also be observed in Fig. 11b that below E_{co}, the imaginary part of the dielectric function increases sharply when the energy decreases. This increase in the IR region comes from the absorption of free-carriers, characteristics of a metal.

At this stage, we decided to fit at the same time the real and imaginary parts of the dielectric function obtained by the point-by-point method with a Tauc Lorentz (TL) model in order to obtain the band gap E_g and to extract the transitions inside the electronic band structure. The Tauc-Lorentz model is well described in the paper by G.E. Jellison and F.A. Modine.[64] To describe the optical properties of VO_2 when the film becomes conductive, a Drude model [65] is added to the TL dispersion model in order to take into account the contribution of free electrons:

$$\varepsilon(\omega) = \varepsilon_r(\infty)\left(1 - \frac{\omega_p^2}{\omega^2 - i\Gamma_d\omega}\right) + \varepsilon_{TL}(\omega) \qquad (4)$$

where $\varepsilon_r(\infty)$ is a constant contribution (larger than unity). The Drude term is characterized by the screened plasma energy ω_p and the damping factor, Γ_d. The

imaginary part of the TL dielectric function is defined as the sum of N TL oscillators according to:

$$\varepsilon_{TLi}(E) = \sum_{0}^{N} \frac{1}{E} \frac{A_i E_i W_i (E - E_g)^2}{(E^2 - E_i^2)^2 + W_i^2 E^2} \quad (5)$$

where A_i is the strength of peak i, E_i its central energy and W_i its width. E_g stands for the optical gap. Each oscillator is assumed to correspond to inter-band transitions in the material sharing a common optical gap E_g. The real part of the dielectric function can be analytically calculated from the Kramers-Kronig integration:

$$\varepsilon_{TLr}(E) = \frac{2}{\pi} P \int_{E_g}^{\infty} \frac{\xi \varepsilon_{TLi}(\xi)}{\xi^2 - E^2} d\xi \quad (6)$$

ξ is the energy parameter of integration (Cauchy's residue theorem) and P stands for the Cauchy principal part of the integral. The derivation of the previous integral gives an analytical expression which is detailed in the work of Jellison and Modine.[64]

The great advantage of this model is to provide quantitative information about the location of the energy bands. We then examined if the E_i energies independently determined by fitting the data with Tauc-Lorentzian oscillators were in agreement with the theoretical model of band structure proposed by Goodenough [66]. Following its notation, we observe (see Fig. 12) that the values of the energy levels in the insulating phase between the filled $d_{\|}$ band and the empty π^* and $d_{\|}^*$ are respectively 1.13 eV and 2.83 eV, as reported in Table 6 in perfect agreement with studies of X-ray Absorption Spectroscopy (XAS) performed by Koethe et al. [67]. The top of the filled O_{2p} (π) band to the middle of the empty π^* band is found to be

equal to 3.49 eV whereas we can attribute the oscillator at 5.28 eV to optical transitions from the filled lower O_{2p} (σ) band to the empty π^* band. To properly describe the appearance of the fitted curves it was necessary to add a component located at 0.58 eV which we can be attributed to the transition at the energy gap E_g which has been estimated to be 0.6 eV.

Table 6. Energy level parameters deduced from the fit to the data using the Tauc-Lorentz model in the insulating and metallic phases. For the description of the symbols used in this table, please refer to their meaning explained in equations 5 and 6.

Parameters (eV)			Monoclinic insulator			Rutile Metal		
A_0	E_0	W_0	27.6	0.58	0.18			
A_1	E_1	W_1	6.59	1.13	0.77			
A_2	E_2	W_2	5.42	2.83	0.9			
A_3	E_3	W_3	12.23	3.49	1.62			
A_4	E_4	W_4	12.14	5.28	3.14			
E_g			0.6					
ε_∞			2.55			3.08		
ω_p						2.08		
Γ_d						0.68		
A_0	E_0	W_0				2.37	2.81	0.72
A_1	E_1	W_1				4.76	3.41	1.19
A_2	E_2	W_2				7.21	4.81	2.01

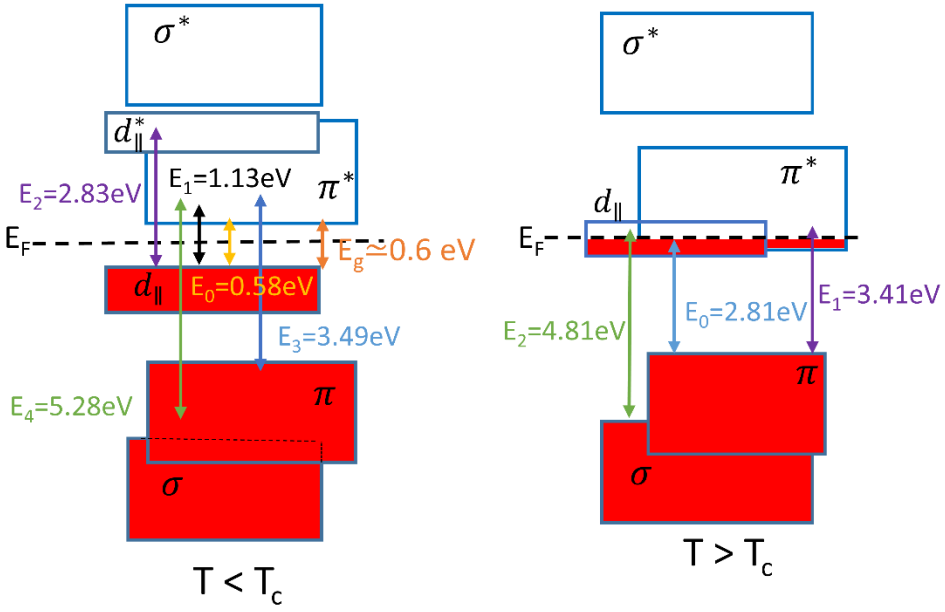

Fig. 12. Schematic energy band illustrating the electronic structure of the metallic (on the right) and insulating (on the left) phases of pure VO_2. The length of the arrows is proportional to the energy of the oscillators. For the description of the symbols used in this table, please refer to their meaning explained in equations 5 and 6.

We find that the screened plasma energy is ω_p =2.08 eV with a broadening factor Γ_d=0.68 eV (see Table 6). This yields an screened plasma frequency ν_p=5.0310^{14} Hz. The broadening parameter corresponds to an average time between collisions of τ = 6.0810^{-15} s. The energies of the Tauc-Lorentzian oscillators in the metallic phase are represented in Fig. 12. We observe that the MIT is accompanied by a reduction of the energy level of the π^* band with respect to the top of the $O_{2p}(\pi)$ band going from 3.49 eV in the insulating phase to 3.41 eV in the metallic phase. A strong reduction is also observed for the transition between the σ and π^* bands (5.28 to 4.81 eV).

3.3 Optical response of W doped $V_{1-x}W_xO_2$ films

Ellipsometric measurements were performed in the same way on W doped thin films to determine the effect of tungsten doping on their optical properties. The real and imaginary parts of the dielectric function at T=25°C from the point by point fit are presented as symbols in Fig. 14. The solid lines represent the adjustment of the dielectric function with the Tauc-Lorentz oscillators. Before discussing the behavior of the dielectric function, we can emphasize the remarkable contribution of the point-by-point adjustment (symbols in Fig. 13) compared to a classic adjustment with a dispersion function (solid line in Fig. 13). Indeed, a notable difference in the real part of the dielectric function at 25°C can be observed when the doping increases. A significant discrepancy is even seen at x=3%. This difference can be explained by the difficulty to correctly model by a dispersion function a material which is not 100% monoclinic at 25°C due to the presence of tungsten (cf. Fig. 6).

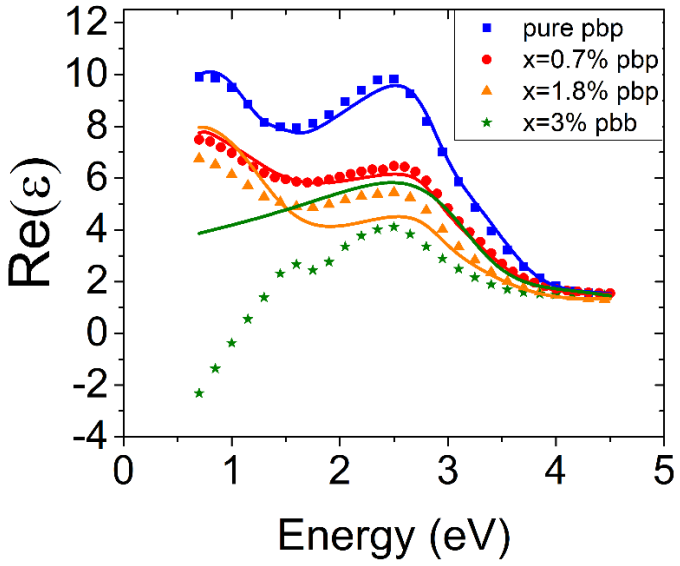

Fig. 13. Evolution of the real part of the dielectric function at T=25°C for x=0%, x=0.7%, x=1.8% and x=3%. The symbols result from the calculation of the dielectric

function deduced from the refractive index calculated by the point-by-point method and the solid lines come from the conventional fitting of the data with a Drude-Lorentz model. It is clear from this Figure that the point-by-point method does not yield similar results especially when the tungsten content increases.

It can be seen in Fig. 14a that the real part is characterized by a decrease in $Re(\varepsilon)$ when the doping percentage x increases. The general shape remains similar except for x=3% for which a metallic behavior characterized by a negative value of the real part of epsilon is clearly visible at 25°C at low energy. The increase in tungsten content affects the local structure around the W dopants which has been identified as a rutile structure even at low doping by X-ray absorption fine structure spectroscopy (XAFS) and X-Ray Diffraction in previous works [23, 56]. Similarly, a drastic modification of the imaginary part of the dielectric function observed at 3% (see Fig. 14b). The imaginary part of the dielectric function is no longer compatible with insulating behavior. In this case, an increase typical of a metallic model of Drude is observed which implies to describe the imaginary part by a sum of Tauc-Lorentz functions with a Drude component. Actually, we have included in the fits of all doped films a Drude component. As shown in Table 7, a very small Drude component at 0.7% and 1.8% characterized by a weak plasma frequency is found. It can therefore be concluded that by increasing the W doping, the film probably consists of a mixed phase containing insulating and metallic domains coexisting at room temperature. Note that this statement is reinforced by the X-ray scattering study presented in Fig. 6 in which it is clear that the percentage of monoclinic phase never reaches 100% when the content of W increases. Further evidence of the phase coexistence is shown in Fig. 14 (see comments related to the arrows in the text). The existence of mixed phases,

when the temperature approaches T_{MIT}, is well described in the article by Nazari et al. [32] for pure VO_2 films deposited on sapphire.

The intersection of the linear part of the dielectric function with the horizontal axis (corresponding to Im(ε) =0 dashed curves in Fig. 14b) gradually decreases when x goes from x=0% to x=1.8%. This value defines the energy gap of the insulating phase. The determination of the gap was further ascertained in the Tauc-Lorentz calculation. The adjusted value of the gap was found to vary from E_g=0.6 eV to E_g=0.2 eV for x=0% and 0.7% respectively. At x=1.8% and T=25°C, the gap was found to be zero showing that the metallic behavior was almost achieved. The decrease of the gap by doping is a behavior already observed. [68]

The amplitude and position of the Tauc-Lorentz parameters are very similar for pure VO_2 (x=0%) and x=0.7% (see Tables 6 and 7). Some trends in the evolution of the transition energies can be observed from Table 7. The difference between the energy levels from the filled lower O2p band (σ) to the empty π* band gradually decreases from 6.47 eV to 4.88 eV as x goes from 0.7% to 3% respectively. Similarly, the transition between the bonding and antibonding $d_{\|}$ orbitals decreases from 2.9 eV to 2.8 eV. This observation is in good agreement with the results of Wu et al [20] studied by XAFS. The substitution of a V^{4+} ion by a W^{6+} ion in the VO_2 unit cell provides two additional electrons, which not only causes the distortion of the nearby monoclinic VO_2 lattice (an increase in electron density), but also a change in the band structure. These effects result in the downward shift of the π* electron band and a smaller separation between the antibonding $d_{\|}^*$ and bonding $d_{\|}$ orbitals in the VO_2 band structure. As a result, the potential energy barrier for the phase transition is lowered as obtained by adjusting the relevant bands. Note that the transition between

the top of the full O_{2p} (π) band and the middle of the empty π^* band located close to 3.5 eV is not affected by the doping, because it is also not impacted by the rise in temperature (see Table 7).

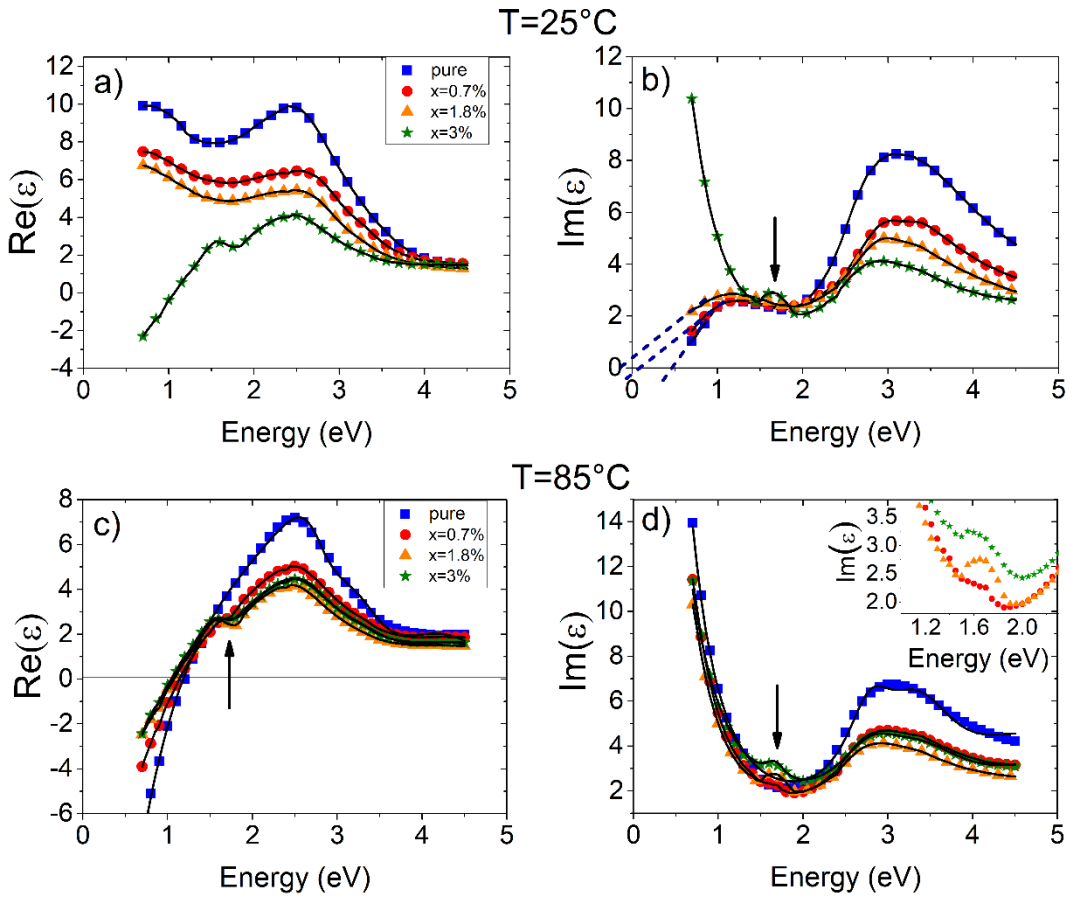

Fig. 14. Evolution of the real part and imaginary part of the dielectric function at a) b) T=25°C for x=0%, x=0.7%, x=1.8% and x=3% and c) d) at T=85°C. The dashed lines in b) give an indication of the evolution of the optical energy gap E_g. The full lines result from a fit to the point by point data with the Tauc-Lorentz model of the dielectric functions. The inset figure in d) is a magnification of the imaginary part of the dielectric function around the energy at 1.6 eV.

Table 7: Fitted Parameters assuming five Tauc Lorentz oscillators to describe the dielectric permittivity at T=25°C and at 85°C for x=0.7% 1.8% and 3%. From left to right are shown the energy gap, the dielectric permittivity ε_∞, the amplitude of the oscillator, its energy E_i and finally its width. Note, we define a screened plasma energy ω_p (whose value is displayed below E_g in brown color) with a broadening factor Γ_d (Drude component) even at 25°C to take into account a possible metallic behavior.

	T = 25°C					T = 85°C				
	E_g(eV) ω_p(eV)	ε_∞ Γ_d (eV)	A	E(eV)	W(eV)	E_g (eV) ω_p(eV)	ε_∞ Γ_d (eV)	A	E(eV)	W(eV)
x=0.7%			4.15	1.23	1.43			0.01	1.68	0.006
	0.24	1.46	1.16	2.89	0.73	0	2.42	1.90	2.81	0.83
	0.35	1.11	6.68	3.43	1.68	2.10	0.80	3.42	3.46	1.32
			16.94	6.47	6.34			5.66	4.99	2.06
x=1.8%			2.11	1.35	1.43			0.16	1.68	0.19
	0	1.57	1.47	2.90	0.90	0	2.23	1.86	2.79	0.89
	0.31	1.32	3.75	3.48	1.72	2.08	0.89	2.85	3.43	1.37
			9.54	5.84	4.73			4.33	4.88	2.07
x=3%			0.21	1.69	0.22			0.23	1.68	0.29
	0	2.24	1.96	2.80	0.93	0	2.20	2.05	2.83	0.97
	2.04	0.91	2.83	3.45	1.39	2.24	0.97	3.48	3.48	1.49
			4.19	4.88	2.03			5.58	5.07	2.19

At T=85°C, all the curves of the dielectric function show a metallic behavior. The variations of the real part of the dielectric function are more pronounced for x=0% than for the other concentrations for which the shape of *Re(ε)* remains fairly similar

(cf. Fig. 14c). One can also notice a slight dip in the real dielectric function below 1.68 eV marked by an arrow in Fig. 14c. As shown in Fig. 14d, the imaginary part of the dielectric function differs by a decrease in its amplitude in the range from 2.5 eV to 4.5 eV with the highest value for x=0% but above all it appears a new peak at 1.68 eV (indicated by an arrow in Fig. 14 b and d) which increases with the percentage of tungsten. This peak was not present in the fits by the Drude-Lorentz method (not shown here). These phenomena observed at 1.68 eV on both the real and imaginary parts of the dielectric function could be explained by the coexistence of a monoclinic phase and a rutile phase even at 85°C (see Fig. 6). A mixture of a monoclinic phase in low proportion in a rutile phase could generate this kind of profile. There is very little change in the plasma energy and in the damping constant as shown in Table 7. This is the signature that the band diagram of the rutile phase does not change much upon doping.

Figs. 15 (a-b) show the variations of the two optical constants *n* and *k* at 1550 nm for different temperatures and concentrations upon heating. We can easily deduce from the two figures the transition temperature upon heating for the four samples. The transition temperature is T_h= 75°C for pure VO_2 and T_h=57°C, 44°C and 39°C for $V_{1-x}W_xO_2$ doped at x=0.7% W, 1.8% W and 3% W respectively. It is thus observed that the transition temperature decreases with increasing tungsten content as already reported in the literature.[25, 48, 69, 70] All these results are in good agreement with those found by XRD (see Fig. 6). We also observe that both the refractive index and the extinction coefficient are affected by doping. A general trend is a decrease of the refraction index in the monoclinic phase as x increases and an increase with x of the extinction coefficient in the rutile phase as shown in Fig. 15.

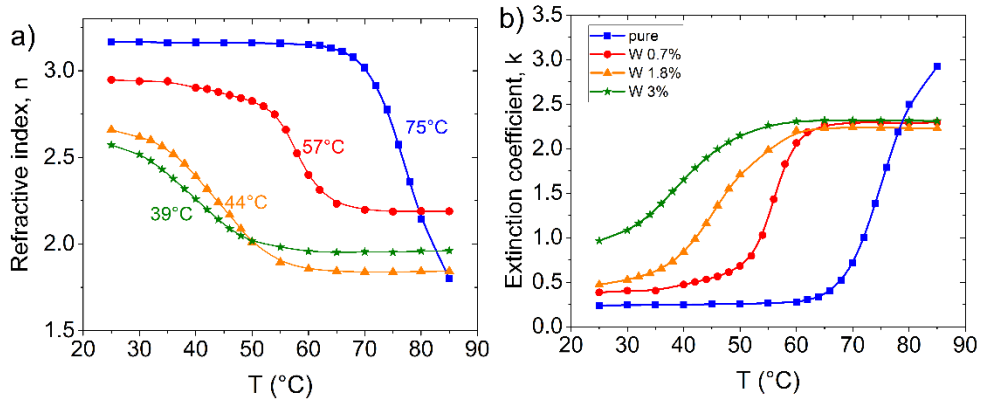

Fig. 15. Variation of the refractive index and of the extinction coefficient for pure VO_2 and tungsten doped (x=[0.7%-1.8%-3%]) VO_2 as a function of temperature at λ=1550 nm**.**

In order to eliminate the influence of the nature of the substrate, the spectral reflectivity and the transmittance of VO_2 free standing films at T=25°C and T=85°C at normal incidence were calculated from the point by point n and k values. The total amplitude of the transmittance and of the reflectance at normal incidence is obtained by adding the amplitudes of the multiple reflections. The phase shift term $\beta = \frac{4\pi(n+ik)h}{\lambda}$ where h is the film thickness, takes into account the path length difference between the incident and reflected beams. It should be noted that the thickness of the free films is much less than the coherence length of the incident beam. Otherwise, it would be necessary to add the intensities and not the amplitudes. In the following, we consider a free standing VO_2 layer of refractive index n and thickness h surrounded by air of refractive index $n = 1$. For the calculation, the thicknesses were set to those reported in Table 3. This leads to the following reflectance and transmittance in amplitude:

$$r = \frac{r_{01} - r_{01}e^{i\beta}}{1 - r_{01}r_{01}e^{i\beta}} \quad and\ t = \frac{t_{01}t_{10}e^{i\beta}}{1 - r_{01}r_{01}e^{i\beta}} \qquad (7)$$

Where r_{01}, t_{01}, t_{10} the amplitudes reflectance and transmittance at the air/film and film/air interfaces:

$$r_{01} = \frac{1 - n - ik}{1 + \mathrm{n} + \mathrm{ik}}\ ,\quad t_{01} = \frac{2}{1 + n + ik}\ ,\ t_{10} = \frac{2(n + ik)}{1 + n + ik} \qquad (8)$$

The intensity transmittance and reflectance at normal incidence in this free standing film are:

$$R = rr^* \quad and \quad T = tt^* \qquad (9)$$

The results are presented in Figure 16. From the high and low temperature transmittance spectra of pure and doped VO_2 thin films (Fig. 16(b) and (d)), TIM is clearly observed as a dramatic change in infrared transmittance with temperature. Going from 25°C to 85°C, the transmittance at 1800 nm drops from 30-60% depending on the doping to 10-30% in agreement with the conductive state of VO_2 at high temperature. We can list the benefits of tungsten doping on the optical properties: (i) At 25°C we are looking for a film with a good transmittance in the infrared range. The best transmittance at 25°C (60%) is observed for the films doped with 0.7% W. It can be noticed that the increase of the percentage of W to 3% in the film does not improve the transmittance (30%) even at low temperature probably due to the coexistence of metallic and insulating phases. (ii) At 85°C the film must reduce the infrared radiation, while having a good transmittance in the visible. Figure 16 shows that the presence of tungsten results in a much higher transmittance in the visible range than that of pure VO_2 film. This could be attributed to the presence of

porosity in the doped VO_2 films improving the visible optical properties of the films [71].

As expected, the reflectivity shows a behavior opposite to the transmittance, except that the roughness and the structure (porosity...) of the film can affect the reflectivity. Hence the reflectivity of pure VO_2 at 25°C appears to be higher than that of doped films.

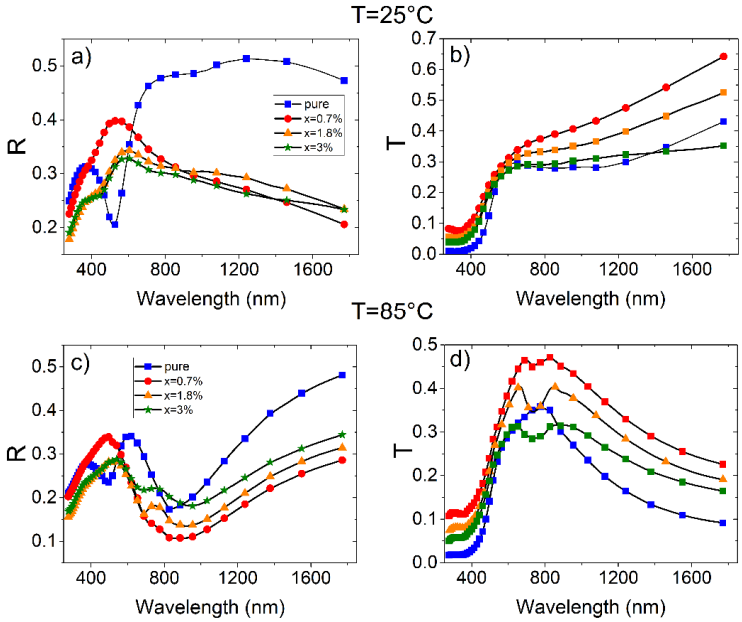

Fig. 16: Calculated reflectivity and transmission at a) b) T=25°C and c) d) T=85°C for a free-standing film of thickness h=70nm.

4. Conclusion

The influence of tungsten doping (x ranging from 0 to 3%) on the structural phase transition and on the optical properties of W-doped thin films is reported as a function of temperature. By monitoring the location of the most intense Bragg peak which transforms from the (110) rutile into the (011) monoclinic phase, we measured the temperature dependent percentage of the monoclinic phase in the films. The increase

in tungsten concentration reveals that the films neither achieve a pure metallic nor a pure insulating behavior. This is attributed to the presence of coexisting domains. We show that the transition temperature T_{MIT} is lowered from 69.6°C for pure VO_2 to 41.6°C for x=3%. We further evidence that the width of the hysteresis is reduced from 8°C to 4°C when x changes form x=0% to x=3% although the film thickness has been divided by almost a factor of 2. This behavior which is opposite to the evolution of the hysteresis of pure VO_2 films with the thickness [42] is attributed to the role of tungsten doping. We also observe that the temperature ranges over which the transition occurs is much broader in doped films. This effect, attributed to phase coexistence, is in perfect agreement with previous observations reported in the literature. [46,48] X-ray reflectivity analysis shows that the thickness of the thin films does not change much through the transition. The increase in tungsten atomic concentration is however associated to an increase of the film roughness.

Ellipsometric spectroscopic measurements of pure and doped films were carried out at two temperatures 25°C and 85°C for pure VO_2. X-ray reflectivity coupled to ellipsometric spectroscopy eliminates any possible correlation between the refractive index and the thickness of the VO_2 films usually encountered in the analysis of ellipsometric data. The calculation of the refractive index n and extinction coefficient k was carried out by either the point by point and the classical Drude Lorentz methods. The results clearly show the efficiency of the point by point method over the Drude Lorentz one especially when the content of tungsten increases. In particular, the optical functions of the tungsten doped film significantly differ when using the point-by-point method from the ones calculated with the Drude-Lorentz model. The biggest deviation is found for the 3% doped sample at 25°C. From these results, the dielectric function of tungsten doped VO_2 thin films was determined. We clearly

show in both X-ray diffraction and ellipsometry analyzes that at higher W doping content a coexistence of rutile and monoclinic phases occurs. An adjustment to the dielectric function by adding a Tauc-Lorentz model and a Drude model allowed us to quantify the energies of the inter-band electronic transitions of the films for the different W doping rates.

Finally, the reflectance and transmittance of free standing films were determined. The 0.7% doped sample was found to be the one having the highest transmittance at 25°C in the infrared region.

Acknowledgements

The authors (AG and MM) gratefully recognize the partial financial support of ADESFA2 under the acronym UMSAMABOT.

CRediT authorship contribution statement
Abdelaziz Ait Abdelkadir: Investigation, Writing – original draft. **Jean-Louis Victor:** Resources **Guillaume Vignaud:** Conceptualization, Methodology, Writing - Review & Editing**,** Formal analysis**,** Supervision**, Corinne Marcel:** Resources**, Sahal Mustapha:** Writing - Review & Editing**, Malik Maaza:** Funding acquisition**, Mohamed Chaker:** Writing - Review & Editing, **Alain Gibaud:** Conceptualization, Methodology, Writing - Review & Editing**,** Formal analysis**,** Supervision**,** Funding acquisition

References

[1] K. Rogers, An X-ray diffraction study of semiconductor and metallic vanadium dioxide, Powder Diffraction, 8 (1993) 240-244.
[2] F. Morin, Oxides which show a metal-to-insulator transition at the Neel temperature, Physical review letters, 3 (1959) 34.
[3] F. Guinneton, L. Sauques, J. Valmalette, F. Cros, J. Gavarri, Comparative study between nanocrystalline powder and thin film of vanadium dioxide VO2: electrical and infrared properties, Journal of Physics and Chemistry of Solids, 62 (2001) 1229-1238.
[4] J. Livage, Optical and electrical properties of vanadium oxides synthesized from alkoxides, Coordination chemistry reviews, 190 (1999) 391-403.

[5] J.K. Kana, J. Ndjaka, G. Vignaud, A. Gibaud, M. Maaza, Thermally tunable optical constants of vanadium dioxide thin films measured by spectroscopic ellipsometry, Optics Communications, 284 (2011) 807-812.
[6] K. Liu, S. Lee, S. Yang, O. Delaire, J. Wu, Recent progresses on physics and applications of vanadium dioxide, Materials Today, 21 (2018) 875-896.
[7] N.B. Aetukuri, A.X. Gray, M. Drouard, M. Cossale, L. Gao, A.H. Reid, R. Kukreja, H. Ohldag, C.A. Jenkins, E. Arenholz, Control of the metal–insulator transition in vanadium dioxide by modifying orbital occupancy, Nature Physics, 9 (2013) 661-666.
[8] G. Stefanovich, A. Pergament, D. Stefanovich, Electrical switching and Mott transition in VO2, Journal of Physics: Condensed Matter, 12 (2000) 8837.
[9] Z. Shao, X. Cao, H. Luo, P. Jin, Recent progress in the phase-transition mechanism and modulation of vanadium dioxide materials, NPG Asia Materials, 10 (2018) 581-605.
[10] Y. Cui, Y. Ke, C. Liu, Z. Chen, N. Wang, L. Zhang, Y. Zhou, S. Wang, Y. Gao, Y. Long, Thermochromic VO2 for energy-efficient smart windows, Joule, 2 (2018) 1707-1746.
[11] J. Outón, A. Casas-Acuña, M. Domínguez, E. Blanco, J.J. Delgado, M. Ramírez-del-Solar, Novel laser texturing of W-doped VO2 thin film for the improvement of luminous transmittance in smart windows application, Applied Surface Science, 608 (2023) 155180.
[12] R. Shi, N. Shen, J. Wang, W. Wang, A. Amini, N. Wang, C. Cheng, Recent advances in fabrication strategies, phase transition modulation, and advanced applications of vanadium dioxide, Applied Physics Reviews, 6 (2019) 011312.
[13] S. Cueff, J. John, Z. Zhang, J. Parra, J. Sun, R. Orobtchouk, S. Ramanathan, P. Sanchis, VO2 nanophotonics, APL Photonics, 5 (2020) 110901.
[14] N. Shen, S. Chen, R. Huang, J. Huang, J. Li, R. Shi, S. Niu, A. Amini, C. Cheng, Vanadium dioxide for thermochromic smart windows in ambient conditions, Materials Today Energy, 21 (2021) 100827.
[15] F. Beteille, J. Livage, Optical switching in VO2 thin films, Journal of Sol-Gel Science and Technology, 13 (1998) 915-921.
[16] R. Pei, X. Ma, C. Han, Z. Liu, Z. Cheng, X. Dong, The valence conversion mechanism for Mo-doped VO2 films with enhanced thermochromic properties, Zeitschrift für anorganische und allgemeine Chemie, (2022) e202200132.
[17] H. Li, J. Wang, Z. You, Y. Yu, P. Li, L. Xiong, Y. He, Nb-doped VO2 thin films with enhanced thermal sensing performance for uncooled infrared detection, Materials Research Bulletin, 146 (2022) 111615.
[18] J. Du, Y. Gao, H. Luo, L. Kang, Z. Zhang, Z. Chen, C. Cao, Significant changes in phase-transition hysteresis for Ti-doped VO2 films prepared by polymer-assisted deposition, Solar Energy Materials and Solar Cells, 95 (2011) 469-475.
[19] A. Krammer, O. Bouvard, A. Schüler, Study of Si doped VO2 thin films for solar thermal applications, Energy Procedia, 122 (2017) 745-750.
[20] A. Krammer, A. Magrez, W.A. Vitale, P. Mocny, P. Jeanneret, E. Guibert, H.J. Whitlow, A.M. Ionescu, A. Schüler, Elevated transition temperature in Ge doped VO2 thin films, Journal of Applied Physics, 122 (2017) 045304.
[21] K. Shibuya, M. Kawasaki, Y. Tokura, Metal-insulator transition in epitaxial V 1− x W x O 2 (0≤ x≤ 0.33) thin films, Applied Physics Letters, 96 (2010) 022102.

[22] T.-L. Wu, L. Whittaker, S. Banerjee, G. Sambandamurthy, Temperature and voltage driven tunable metal-insulator transition in individual W x V 1− x O 2 nanowires, Physical Review B, 83 (2011) 073101.
[23] Y. Wu, L. Fan, W. Huang, S. Chen, S. Chen, F. Chen, C. Zou, Z. Wu, Depressed transition temperature of W x V 1− x O 2: mechanistic insights from the X-ray absorption fine structure (XAFS) spectroscopy, Physical Chemistry Chemical Physics, 16 (2014) 17705-17714.
[24] S. Liang, Q. Shi, H. Zhu, B. Peng, W. Huang, One-step hydrothermal synthesis of W-doped VO2 (M) nanorods with a tunable phase-transition temperature for infrared smart windows, ACS omega, 1 (2016) 1139-1148.
[25] S. Dou, W. Zhang, Y. Wang, Y. Tian, Y. Wang, X. Zhang, L. Zhang, L. Wang, J. Zhao, Y. Li, A facile method for the preparation of W-doped VO2 films with lowered phase transition temperature, narrowed hysteresis loops and excellent cycle stability, Materials chemistry and physics, 215 (2018) 91-98.
[26] X. Tan, T. Yao, R. Long, Z. Sun, Y. Feng, H. Cheng, X. Yuan, W. Zhang, Q. Liu, C. Wu, Unraveling metal-insulator transition mechanism of VO 2 triggered by tungsten doping, Scientific reports, 2 (2012) 1-6.
[27] L. Chen, C. Huang, G. Xu, L. Miao, J. Shi, J. Zhou, X. Xiao, Synthesis of thermochromic W-doped VO2 (M/R) nanopowders by a simple solution-based process, Journal of nanomaterials, 2012 (2012).
[28] L. Hu, H. Tao, G. Chen, R. Pan, M. Wan, D. Xiong, X. Zhao, Porous W-doped VO2 films with simultaneously enhanced visible transparency and thermochromic properties, Journal of Sol-Gel Science and Technology, 77 (2016) 85-93.
[29] E. Shin, K. Pan, W. Wang, G. Subramanyam, V. Vasilyev, K. Leedy, T. Quach, Tungsten-doped vanadium dioxide thin film based tunable antenna, Materials Research Bulletin, 101 (2018) 287-290.
[30] H.J. Kim, Y.H. Choi, D. Lee, I.H. Lee, B.K. Choi, S.-H. Phark, Y.J. Chang, Enhanced passive thermal stealth properties of VO2 thin films via gradient W doping, Applied Surface Science, 561 (2021) 150056.
[31] J.M. Booth, P.S. Casey, Anisotropic structure deformation in the VO 2 metal-insulator transition, Physical review letters, 103 (2009) 086402.
[32] F. Grandi, A. Amaricci, M. Fabrizio, Unraveling the Mott-Peierls intrigue in vanadium dioxide, Physical Review Research, 2 (2020) 013298.
[33] J.K. Kana, G. Vignaud, A. Gibaud, M. Maaza, Thermally driven sign switch of static dielectric constant of VO2 thin film, Optical Materials, 54 (2016) 165-169.
[34] H. Kakiuchida, P. Jin, S. Nakao, M. Tazawa, Optical properties of vanadium dioxide film during semiconductive–metallic phase transition, Japanese Journal of Applied Physics, 46 (2007) L113.
[35] J. Sun, G.K. Pribil, Analyzing optical properties of thin vanadium oxide films through semiconductor-to-metal phase transition using spectroscopic ellipsometry, Applied Surface Science, 421 (2017) 819-823.
[36] C. Wan, Z. Zhang, D. Woolf, C.M. Hessel, J. Rensberg, J.M. Hensley, Y. Xiao, A. Shahsafi, J. Salman, S. Richter, On the optical properties of thin-film vanadium dioxide from the visible to the far infrared, Annalen der Physik, 531 (2019) 1900188.
[37] M. Nazari, Y. Zhao, V.V. Kuryatkov, Z. Fan, A.A. Bernussi, M. Holtz, Temperature dependence of the optical properties of VO 2 deposited on sapphire with different orientations, Physical Review B, 87 (2013) 035142.

[38] J. Ramirez-Rincon, C. Gomez-Heredia, A. Corvisier, J. Ordonez-Miranda, T. Girardeau, F. Paumier, C. Champeaux, F. Dumas-Bouchiat, Y. Ezzahri, K. Joulain, Thermal hysteresis measurement of the VO2 dielectric function for its metal-insulator transition by visible-IR ellipsometry, Journal of Applied Physics, 124 (2018) 195102.
[39] J. Hilfiker, R. Synowicki, H. Tompkins, Spectroscopic ellipsometry methods for thin absorbing coatings, in: Society of Vacuum Coaters. Proceedings 51st Annual Technical Conference, 2008, pp. 511-516.
[40] M. Gilliot, A. Hadjadj, M. Stchakovsky, Revised wavelength-by-wavelength inversion of ellipsometry data of semiconductor thin films, Journal of Vacuum Science & Technology B, Nanotechnology and Microelectronics: Materials, Processing, Measurement, and Phenomena, 37 (2019) 062925.
[41] J.-L. Victor, C. Marcel, L. Sauques, C. Labrugère, F. Amiard, A. Gibaud, A. Rougier, From multilayers to V1-xWxO2±δ films elaborated by magnetron sputtering for decreasing thermochromic transition temperature, Journal of Alloys and Compounds, 858 (2021) 157658.
[42] G. Vignaud, A. Gibaud, REFLEX: a program for the analysis of specular X-ray and neutron reflectivity data, Journal of Applied Crystallography, 52 (2019) 201-213.
[43] A. Gibaud, G. Vignaud, S. Sinha, The correction of geometrical factors in the analysis of X-ray reflectivity, Acta Crystallographica Section A: Foundations of Crystallography, 49 (1993) 642-648.
[44] A. Gibaud, G. Vignaud, Specular reflectivity from smooth and rough surfaces, in: X-ray and Neutron Reflectivity, Springer, 2009, pp. 85-131.
[45] L. Lutterotti, Maud: a Rietveld analysis program designed for the internet and experiment integration, Acta Crystallogr. A, 56 (2000) s54.
[46] R. Zhang, Q. Fu, C. Yin, C. Li, X. Chen, G. Qian, C. Lu, S. Yuan, X. Zhao, H. Tao, Understanding of metal-insulator transition in VO 2 based on experimental and theoretical investigations of magnetic features, Scientific reports, 8 (2018) 1-7.
[47] R. Basu, V. Srihari, M. Sardar, S.K. Srivastava, S. Bera, S. Dhara, Probing phase transition in VO 2 with the novel observation of low-frequency collective spin excitation, Scientific reports, 10 (2020) 1-11.
[48] Y. Huang, D. Zhang, Y. Liu, J. Jin, Y. Yang, T. Chen, H. Guan, P. Fan, W. Lv, Phase transition analysis of thermochromic VO2 thin films by temperature-dependent Raman scattering and ellipsometry, Applied Surface Science, 456 (2018) 545-551.
[49] T. Cesca, C. Scian, E. Petronijevic, G. Leahu, R.L. Voti, G. Cesarini, R. Macaluso, M. Mosca, C. Sibilia, G. Mattei, Correlation between in situ structural and optical characterization of the semiconductor-to-metal phase transition of VO 2 thin films on sapphire, Nanoscale, 12 (2020) 851-863.
[50] E. Gagaoudakis, E. Aperathitis, G. Michail, M. Panagopoulou, D. Katerinopoulou, V. Binas, Y. Raptis, G. Kiriakidis, Low-temperature rf sputtered VO2 thin films as thermochromic coatings for smart glazing systems, Solar Energy, 165 (2018) 115-121.
[51] E. Shadrin, A. Il'inskiĭ, A. Sidorov, S. Khanin, Size effects upon phase transitions in vanadium oxide nanocomposites, Physics of the Solid State, 52 (2010) 2426-2433.
[52] D. Brassard, S. Fourmaux, M. Jean-Jacques, J. Kieffer, M. El Khakani, Grain size effect on the semiconductor-metal phase transition characteristics of magnetron-sputtered VO 2 thin films, Applied Physics Letters, 87 (2005) 051910.

[53] A. Yano, H. Clarke, D.G. Sellers, E.J. Braham, T.E. Alivio, S. Banerjee, P.J. Shamberger, Toward high-precision control of transformation characteristics in VO2 through dopant modulation of hysteresis, The Journal of Physical Chemistry C, 124 (2020) 21223-21231.
[54] N. Shen, S. Chen, R. Shi, S. Niu, A. Amini, C. Cheng, Phase Transition Hysteresis of Tungsten Doped VO2 Synergistically Boosts the Function of Smart Windows in Ambient Conditions, ACS Applied Electronic Materials, 3 (2021) 3648-3656.
[55] J. Li, W. Liu, X. Zhang, P.K. Chu, K.M. Cheung, K.W. Yeung, Temperature-responsive tungsten doped vanadium dioxide thin film starves bacteria to death, Materials Today, 22 (2019) 35-49.
[56] K. Mulchandani, A. Soni, K. Pathy, K. Mavani, Structural transformation and tuning of electronic transitions by W-doping in VO2 thin films, Superlattices and Microstructures, 154 (2021) 106883.
[57] C. Tang, P. Georgopoulos, M. Fine, J. Cohen, M. Nygren, G. Knapp, A. Aldred, Local atomic and electronic arrangements in W x V 1− x O 2, Physical Review B, 31 (1985) 1000.
[58] N. Émond, Synthèse et caractérisation de couches minces de VO_2 et de $W_xV_{1-x}O_2$ pour des applications dans les domaines infrarouge et térahertz, in, Université du Québec, Institut national de la recherche scientifique, 2017.
[59] M. Di, E. Bersch, A.C. Diebold, S. Consiglio, R.D. Clark, G.J. Leusink, T. Kaack, Comparison of methods to determine bandgaps of ultrathin HfO2 films using spectroscopic ellipsometry, Journal of Vacuum Science & Technology A: Vacuum, Surfaces, and Films, 29 (2011) 041001.
[60] T. Chang, X. Cao, L.R. Dedon, S. Long, A. Huang, Z. Shao, N. Li, H. Luo, P. Jin, Optical design and stability study for ultrahigh-performance and long-lived vanadium dioxide-based thermochromic coatings, Nano Energy, 44 (2018) 256-264.
[61] T. Peterseim, M. Dressel, M. Dietrich, A. Polity, Optical properties of VO2 films at the phase transition: Influence of substrate and electronic correlations, Journal of Applied Physics, 120 (2016) 075102.
[62] M. Jiang, Y. Li, S. Li, H. Zhou, X. Cao, S. Bao, Y. Gao, H. Luo, P. Jin, Room temperature optical constants and band gap evolution of phase pure M1-VO2 thin films deposited at different oxygen partial pressures by reactive magnetron sputtering, Journal of Nanomaterials, 2014 (2014).
[63] M. Kang, S.W. Kim, J.-W. Ryu, T. Noh, Optical properties for the Mott transition in VO2, Aip Advances, 2 (2012) 012168.
[64] G. Jellison Jr, F. Modine, Parameterization of the optical functions of amorphous materials in the interband region, Applied Physics Letters, 69 (1996) 371-373.
[65] H. Sehmi, W. Langbein, E. Muljarov, Optimizing the Drude-Lorentz model for material permittivity: Method, program, and examples for gold, silver, and copper, Physical Review B, 95 (2017) 115444.
[66] J.B. Goodenough, The two components of the crystallographic transition in VO2, Journal of Solid State Chemistry, 3 (1971) 490-500.
[67] T. Koethe, Z. Hu, M. Haverkort, C. Schüßler-Langeheine, F. Venturini, N. Brookes, O. Tjernberg, W. Reichelt, H. Hsieh, H.-J. Lin, Transfer of Spectral Weight and Symmetry across the Metal-Insulator Transition in VO 2, Physical review letters, 97 (2006) 116402.

[68] A.S. Hassanien, I. Sharma, K.A. Aly, Linear and nonlinear optical studies of thermally evaporated chalcogenide a-Pb-Se-Ge thin films, Physica B: Condensed Matter, 613 (2021) 412985.
[69] Y. Yang, X. Cao, G. Sun, S. Long, T. Chang, X. Li, P. Jin, Transmittance change with thickness for polycrystalline VO2 films deposited at room temperature, Journal of Alloys and Compounds, 791 (2019) 648-654.
[70] L. Whittaker, T.-L. Wu, C.J. Patridge, G. Sambandamurthy, S. Banerjee, Distinctive finite size effects on the phase diagram and metal–insulator transitions of tungsten-doped vanadium (iv) oxide, Journal of Materials Chemistry, 21 (2011) 5580-5592.
[71] N.R. Mlyuka, G.A. Niklasson, C.G. Granqvist, Thermochromic VO2-based multilayer films with enhanced luminous transmittance and solar modulation, physica status solidi (a), 206 (2009) 2155-2160.